Check for updates

Sulfonated hierarchical ZSM-5 zeolite monoliths as solid acid catalyst for esterification of oleic acid†

Binhang Zhao, Pan Yang, Nan Zhang, Donald R. Inns, [ID] Elena F. Kozhevnikova, Alexandros P. Katsoulidis, Ivan V. Kozhevnikov, [ID] Alexander Steiner [ID] and Haifei Zhang [ID] *

Sulfonated hierarchical H-ZSM-5 monoliths were synthesized *via* ice-templating as solid acid catalysts for biodiesel production. Characterization confirmed successful −SO₃ group grafting, increasing acid density. The catalysts achieved over 90% conversion of oleic acid in esterification, with easy recovery and reuse, and the relationship between porosity and acid density was explored.

Acid catalysts are widely used in organic reactions, but homogeneous catalysts like H_2SO_4 have limitations, such as separation difficulties, lack of reusability, and equipment corrosion.[1] To address these challenges, researchers focus on developing heterogeneous solid-acid catalysts like zeolites, known for their natural acidity and large surface area.[2,3] Zeolites are particularly useful due to their aluminosilicate structure, which provides catalytic sites that can be enhanced by modifying aluminium content or grafting functional groups.[4]

Sulfonated zeolites have been shown to exhibit high catalytic activity,[5] but their traditional powder form lacks stability in industrial processes, causing issues such as pressure drop, mass transfer, and recovery.[6] Monolithic zeolite structures present a promising approach due to their advantages of high efficiency, ease of recovery, and minimal catalyst loss.[7] Li *et al.* fabricated H-ZSM-5 and HY monoliths, which showed greater stability in *n*-hexane cracking and higher selectivity to light olefins than their powder counterpart.[8] Chai *et al.* produced Cr–Mn bimetallic functionalized USY zeolite monolithic catalyst, demonstrating high catalytic performance for the production of 2,5-furandicarboxylic acid from raw biomass with good recyclability.[6]

In this work, we present a novel approach to synthesising sulfonated hierarchical ZSM-5 monoliths. The macropores were introduced by ice-templating, while the mesopores were formed through the use of cetyltrimethylammonium bromide (CTAB) micelle templating.[9,10] The fabricated zeolite monoliths were further treated with nitric acid to increase the amount of silanol groups,[11] to enhance subsequent grafting of 3-mercaptopropyltrimethoxysilane (3-MPTMS) and sulfonation by oxidizing −SH groups. The resulting sulfonated hierarchical ZSM-5 monoliths exhibited high acidity and improved catalytic performance in the esterification of oleic acid with methanol (Scheme S1, ESI†). Furthermore, the monolithic form of the catalyst showed easy recovery and good recyclability.

The morphology of the catalysts was investigated by scanning electron microscopy (SEM). During the freezing process, water was frozen to form ice crystals, and the NH_4-ZSM-5 particles, along with polyvinyl alcohol (PVA) molecules, were excluded from the freezing front. This caused the zeolite particles and PVA to aggregate between the ice crystals, which, upon sublimation during the freeze-drying process, resulted in the formation of macropores within the monolith. The PVA played a crucial role as a stabilizer by preventing the zeolite particles from settling before freezing, and also acted as a sacrificial binder that held the particles together to form a cohesive monolith. Without PVA, the monoliths were fragile or disintegrated and no stable monoliths could be formed.

SEM images (Fig. 1) confirmed the formation of aligned macropores in the monoliths. The images showed that the NH_4-ZSM-5 particles were evenly distributed and that the macroporous structure was formed after freeze-drying (Fig. 1b). The freeze-dried zeolite monoliths were treated with tetraethyl orthosilicate (TEOS) sol to form silica coating around zeolite particles. This silica coating, particularly after calcination, enhanced the mechanical stability of the monoliths. The aligned structure remained intact after the silica coating process (Fig. 1c) and no significant morphological changes, *i.e.*, aligned macropores, were observed after the sulfonation treatment (Fig. 1d). The presence of aligned macropores is critical for enhancing molecular diffusion and catalytic efficiency.

Department of Chemistry, University of Liverpool, Crown Street, Liverpool L69 7ZD, UK. E-mail: zhanghf@liverpool.ac.uk

† Electronic supplementary information (ESI) available: Experimental procedures, additional characterization and catalysis results. See DOI: https://doi.org/10.1039/d4cc05044d
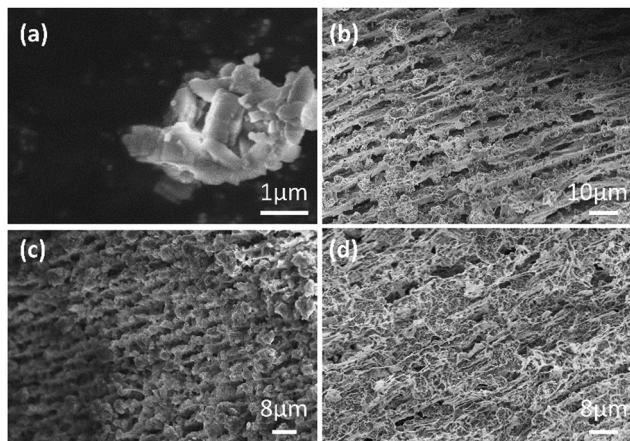
Fig. 1 SEM images of zeolite particles and monoliths. (a) NH$_4$-ZSM-5 particle. (b) Freeze-dried NH$_4$-ZSM-5 monolith. (c) Non-sulfonated monolith H-0.5-Z. (d) Sulfonated monolith H-0.6-SO$_3$-0.5-Z. The prepared zeolite monoliths were named in the form of H-A-SO$_3$-B-Z, where: H indicates treatment with HNO$_3$, A specifies the mass ratio of 3-MPTMS to monoliths and always appear with SO$_3$, B denotes CTAB concentrations (M), Z stands for zeolite.

The X-ray diffraction (XRD) patterns of the parent ZSM-5 particles and the modified ZSM-5 zeolites showed the presence of crystalline zeolite particles (Fig. S1, ESI†). The characteristic diffraction peaks of the parent ZSM-5 corresponded to the MFI framework structure. After the sulfonation treatment, the SO$_3$-ZSM-5 particles retained the characteristic peaks of the parent ZSM-5, with only a slight reduction in peak intensity. This suggests that the sulfonation process did not introduce new phases or alter the crystalline structure of ZSM-5. Notably, no new peaks related to sulfonate groups appeared, indicating that the sulfonate functionalization was successfully dispersed within the zeolite structure without disrupting its framework.[12]

The decrease in intensity of the XRD peaks after coating the parent ZSM-5 with SiO$_2$ was more pronounced, indicating a reduction in crystallinity. This observation could be attributed to the presence of amorphous silica on the zeolite monolith. Nevertheless, the characteristic peaks of the MFI structure remain prominent even after silica coating, suggesting that the fabricated ZSM-5 monoliths retained their ZSM-5 structure.

FTIR spectroscopy (Fig. S2, ESI†) was employed to characterize the modifications of zeolite monoliths. Strong absorption bands near 1050 cm^{-1}, corresponding to the asymmetric stretching vibrations of SiO$_4$ or AlO$_4$ tetrahedra, were observed in all samples. A peak around 790 cm^{-1} was associated with the symmetric stretching of O–Si–O bonds.[13] The increase in the intensity of these bands after treatment with TEOS sol and sulfonation indicated that the silica content in the monoliths had increased.

Moreover, the FTIR spectra showed the presence of O–H stretching vibrations in the range of 3500–3300 cm^{-1}, confirming the presence of –OH groups and qualitative increase in intensity following silica coating and sulfonation (Fig. S2, ESI†).[13] It is difficult to quantify the strength of –OH groups from the FTIR data. The subsequent KOH titration and

NH$_3$–TPD (temperature programmed desorption) analysis provided evidence of total acid density and the differentiation of Si–OH and SO$_3$H group when discussing the catalytic performance below. Although the characteristic S=O stretching vibrations, typically appearing near 1050 cm^{-1} and 1170 cm^{-1}, were not distinguishable due to overlap with the ZSM-5 framework bands,[14] the presence of sulfonic acid groups was confirmed by the detection of a C–S stretching vibration peak at around 690 cm^{-1}.[15] Weak peaks at 1460 cm^{-1} and 2930 cm^{-1} were also observed, corresponding to the asymmetric stretching vibrations of alkyl groups originating from 3-MPTMS,[16] further confirming successful grafting of the sulfonic acid precursor onto the ZSM-5 zeolite. The intensity of these peaks increased with higher concentrations of 3-MPTMS, indicating that the grafting was more extensive in samples with higher loading of the functionalizing agent.

X-ray photoelectron spectroscopy (XPS) analysis was conducted to determine the surface chemical composition and sulphur oxidation states before and after the oxidation process (Fig. 2a and Fig. S3, ESI†). The monolith treated with 3-MPTMS exhibited a doublet peak at 163.4 eV, characteristic of thiol (–SH) groups. Post-oxidation, a new doublet peak emerged at 168.4 eV, while the thiol peak disappeared, indicating the successful conversion to sulfonic acid (–SO$_3$H) groups (Fig. 2a).[17] No significant changes in other surface elements (such as C, Si) were detected after oxidation (Fig. S3, ESI†), confirming the effective transformation of thiol to sulfonic acid groups through the sulfonation process.

Nitrogen adsorption–desorption isotherms (Fig. 2b) were obtained before and after modification. The parent ZSM-5 particles exhibited a typical type I isotherm, with a steep nitrogen uptake at low relative pressures, indicative of a predominantly microporous structure.[18] The presence of a hysteresis loop at higher relative pressures suggested the existence of mesopores,[19] likely formed by the aggregation of small ZSM-5 crystallites. After coating with silica, the surface area of the non-sulfonated ZSM-5 monolith (0-Z) decreased due to the micropores being partially obstructed by the amorphous silica layer. However, in samples treated with CTAB, such as 0.5-Z and 0.8-Z (Fig. S4a, ESI†), the surface area significantly increased due to the formation of mesopores, resulted from the CTAB micelles after calcination. For sulfonated ZSM-5, the
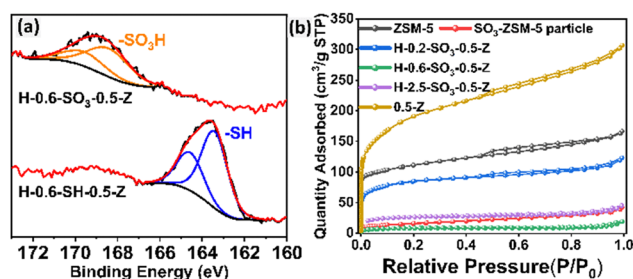
Fig. 2 Characterization of ZSM-5 zeolite materials. (a) XPS spectrum of H-0.6-SO$_3$-0.5-Z and H-0.6-SH-0.5-Z (b) N$_2$ adsorption–desorption isotherms of ZSM-5 particles and monoliths.

Table 1 The surface areas, acid density, and turnover frequency (TOF) of ZSM-5 particles and monoliths

Catalyst	$^aS_{BET}$ (m^2 g^{-1})	$^bS_{micro-BET}$ (m^2 g^{-1})	$^bS_{meso-BET}$ (m^2 g^{-1})	^{c}–SO$_3$ density (mmol g^{-1})	^{d}Total acid density (mmol g^{-1})	^{e}TOF (h^{-1})
^{f}Parent ZSM-5	408	303	105	0	0.46	1.7
SO$_3$-ZSM-5 particle	53	2	51	0.47	0.97	2.4
H-0.2-SO$_3$-0-Z	38	0	38	0.37	0.81	10.8
H-0.2-SO$_3$-0.5-Z	306	120	186	0.33	0.84	8.7
H-0.2-SO$_3$-0.8-Z	465	180	285	0.34	0.89	11.9
H-0.6-SO$_3$-0.5-Z	21	11	10	1.12	1.58	9.8
H-2.5-SO$_3$-0-Z	14	0.5	13.5	0.57	1.14	9.4
H-2.5-SO$_3$-0.5-Z	71	30	41	0.9	1.55	10.5
H-2.5-SO$_3$-0.8-Z	19	0	19	1.19	1.92	8.7
0.2-SO$_3$-0.5-Z	333	98	235	0.31	0.73	10.4

^{a} BET method applied to the N$_2$ isothermal (p/p_0 0.05–0.3). ^{b} Surface area of micropores and mesopores by t-plot method. ^{c} Based on elemental analysis. ^{d} Based on NaOH titration. ^{e} Based on the oleic acid conversion in the first hour of the reaction. ^{f} H-ZSM-5 particle (NH$_4$-ZSM-5 particle after calcination).

nitrogen adsorption isotherms showed a reduction in BET surface area after sulfonation, with the SO$_3$-ZSM-5 particles experiencing a decrease from 408 m^2 g^{-1} to 53 m^2 g^{-1} (Table 1 and Fig. 2b). This sharp decline was attributed to the grafted sulfonic acid groups blocking nearly all the micropores within the ZSM-5 particles instead of structural change of the zeolite particles (Fig. S1, ESI†). This trend became more significant for the sulfonated monoliths, particularly when the zeolite monoliths were grafted with high concentration of 3-MPTMS and subsequently oxidized (Table 1). In this case, a high percentage of mesopores were also blocked (*e.g.*, H-2.5-SO$_3$-0.8-Z). Despite the decrease in surface area, the hierarchical structure of the sulfonated monoliths still allowed for sufficient diffusion pathways, particularly in samples like H-0.2-SO$_3$-0.5-Z and H-0.2-SO$_3$-0.8-Z where the mesopores remained largely intact, leading to a relatively high surface area of 306 m^2 g^{-1} and 465 m^2 g^{-1} (Table 1 and Fig. S4b, d, ESI†) compared to the other sulfonated samples. The acid density of sulfonated samples also had a significant increase after the sulfonation process.

Thermal stability of parent and modified zeolite samples was examined by thermogravimetric analysis (TGA) (Fig. S5, ESI†). Non-sulfonated samples, including parent ZSM-5 and 0.5-Z, exhibited mass loss between 30 °C and 180 °C due to moisture, with 0.5-Z absorbing more water due to its larger surface area and mesopores. Sulfonated samples showed mass loss between 280 °C and 570 °C from decomposition of sulfonic acid groups. SO$_3$-ZSM-5 had lower mass loss compared to the monoliths, indicating fewer sulfonic groups present. Higher 3-MPTMS concentrations increased sulfonic group grafting, but after the mass ratio of 0.6 g g^{-1} to zeolite monolith, further grafting was minimal, indicating grafting saturation.

The catalysts were evaluated by the esterification of oleic acid with methanol. The only product of this reaction was methyl oleate (Fig. S6, ESI†). The non-sulfonated ZSM-5 monoliths exhibited moderate catalytic performance (Fig. S7, ESI†). The conversion of oleic acid increased from 27.4% to 45.8% within 5 h as the CTAB concentration was raised from 0 to 0.8 M. This was because higher CTAB concentrations led to the formation of more mesopores (Table S1, ESI†), which facilitated mass transfer of reactant molecules and improved the catalytic performance. However, the catalytic performance of the

non-sulfonated monoliths remained limited due to low acid site density.

In contrast, sulfonated monoliths showed significantly higher catalytic efficiency (Fig. 3a). Among them, the H-0.6-SO$_3$-0.5-Z monolith exhibited superior performance compared to the SO$_3$-ZSM-5 particles (Fig. 3a), primarily due to its higher acid density and macroporous structure. The monoliths treated with 0.6 g g^{-1} and 2.5 g g^{-1} of 3-MPTMS showed similar performance due to comparable acid densities (Table 1), while the monolith treated with 0.2 g g^{-1} had lower performance, but still higher than sulfonated ZSM-5 particles. The turnover frequency (TOF) for sulfonated ZSM-5 particles was 2.4 h^{-1} whilst higher TOFs were achieved for the monoliths, *e.g.*, 9.8 h^{-1} for H-0.6-SO$_3$-0.5-Z (Table 1). The higher catalytic performance could be attributed to higher acid density (Table 1), which was also confirmed by NH$_3$-TPD analysis, with the sulfonated monolith showing NH$_3$ adsorbed at 7.5 mmol g^{-1} (compared to 5.0 mmol g^{-1} for SO$_3$-ZSM-5 particles) (Table S2, ESI†). The NH$_3$-TPD profile exhibited large peaks at 100–200 °C non-sulfonated samples (which could be attributed to weak acid sites such as Si–OH[20]) and much larger peaks at 200–450 °C for sulfonated samples, indicating enhanced presence of strong acid sites (likely to be –SO$_3$H in
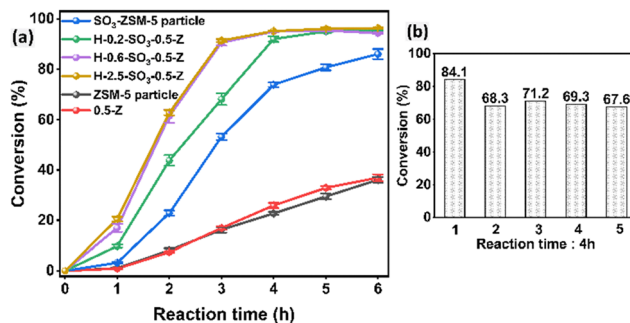
Fig. 3 Conversion rate of oleic acid with methanol using sulfonated zeolite monoliths as catalysts. (a) The sulfonated monolith catalysts compared with ZSM-5 particles and the non-sulfonated zeolite monolith. (b) Reuse of the sulfonated monolith catalyst H-0.2-SO$_3$-0.5-Z for five cycles. Reaction conditions: temperature 120 °C, catalyst loading: 5 wt%, molar ratio of methanol and oleic acid 10 : 1.

this study, Fig. S8, ESI†). The larger peak moved further to higher temperatures for the sulfonated zeolite monolith (Fig. S8, ESI†), suggesting a higher density of strong acid sites, which could explain the better catalytic performance for sulfonated zeolite monoliths.

Other reaction parameters were also investigated. The treatment of zeolite monoliths with HNO_3 led to a slight improvement due to improved grafting of 3-MPTMS (Fig. S9a, ESI†). This treatment could remove Al species (detectable by inductively coupled plasma analysis). The XPS analysis of sulfonated zeolites only showed negligible presence of Al species. The concentrations of CTAB added (0, 0.5, and 0.8 M) were varied to investigate the effect on catalytic performance. For the monoliths treated with 0.2 g g^{-1} 3-MPTMS (Fig. S9b, ESI†), higher CTAB concentrations improved the conversion rate. For the monoliths treated with 2.5 g g^{-1}, all three samples exhibited low surface areas (Table 1), limiting the influence of porosity on catalytic performance. The conversion performance showed a similar trend, *i.e.*, higher CTAB concentration leading to higher conversion of oleic acid (Fig. S9c, ESI†). However, the difference in conversion performance was smaller, compared with the monoliths treated with 0.2 g g^{-1} 3-MPTMS (Fig. S9b, ESI†). The reaction temperature and catalyst loading were then assessed for the same catalyst. Catalytic performance was enhanced with increasing reaction temperatures (90 °C, 120 °C and 150 °C) (Fig. S10a, ESI†) and catalyst loadings (1 wt%, 5 wt% and 10 wt%) (Fig. S10b, ESI†). Both acid density and catalyst structure, including porosity and surface area, are crucial for catalytic efficiency.

Further tests were conducted to assess the stability and recyclability of the sulfonated hierarchical ZSM-5 monoliths. This was demonstrated with the sulfonated zeolite monolith H-0.2-SO$_3$-0.5-Z. After five reaction cycles, the catalyst retained most of its catalytic activity (conversion changed from *ca.* 84% to 68%) (Fig. 3b). There is a larger decrease of conversion from 1st reaction to the 2nd re-cycle reaction, which was attributed to the leaching of unstable grafted acid groups from the monolithic catalyst in the first run. The crystallinity, functionality and structural integrity of the monolith catalyst after 5 cycles of reaction were preserved (Fig. S11–S14, ESI†).

The performance of our sulfonated zeolite monoliths was compared with other modified zeolite catalysts for esterification reactions in literature (Table S3, ESI†). The sulfonated hierarchical ZSM-5 monoliths outperformed other reported zeolites in terms of short reaction time for higher conversion of oleic acid and showed good recyclability.

In conclusion, sulfonated hierarchical ZSM-5 monoliths were prepared *via* ice-templating and subsequent modifications. The hierarchical zeolite monoliths with sulfonic acid groups resulted in improved mass transfer, higher acid site density, and enhanced overall catalytic efficiency. The monolithic form of the catalyst also facilitated easy recovery and

minimized catalyst loss, making these materials well-suited for potential industrial applications, particularly in processes like biodiesel production and oleic acid esterification.

Data availability

The data supporting this article have been included as part of the ESI.†

Conflicts of interest

There are no conflicts to declare.

Notes and references

1 A. Mukhtar, S. Saqib, H. Lin, M. U. H. Shah, S. Ullah, M. Younas, M. Rezakazemi, M. Ibrahim, A. Mahmood, S. Asif and A. Bokhari, *Renew. Sustainable Energy Rev.*, 2022, **157**, 112012.
2 Y.-L. Ding, H.-Q. Wang, M. Xiang, P. Yu, R.-Q. Li and Q.-P. Ke, *Front. Chem.*, 2020, **8**, 790.
3 S. Mardiana, N. J. Azhari, T. Ilmi and G. T. Kadja, *Fuel*, 2022, **309**, 122119.
4 P. H. Hoang, N. H. Chung and L. Q. Dien, *J. Iran. Chem. Soc.*, 2019, **16**, 2203–2210.
5 A. J. Saviola, K. Wijaya, W. D. Saputri, L. Hauli, A. K. Amin, H. Ismail, B. Budhijanto, W.-C. Oh, W. Wangsa and P. Prastyo, *Appl. Nanosci.*, 2023, **13**, 6575–6589.
6 Y. Chai, M. Bai, A. Chen, J. Yuan, C. Peng, D. Zhao, B. Yan and P. Qin, *Chem. Eng. J.*, 2022, **429**, 132173.
7 J. Chen, F. Liu, Y. Li, Y. Dou, S. Liu and L. Xiao, *R. Soc. Open Sci.*, 2020, 7, 200981.
8 X. Li, W. Li, F. Rezaei and A. Rownaghi, *Chem. Eng. J.*, 2018, **333**, 545–553.
9 M. Zhang, J. Lidder, M. Bahri and H. Zhang, *Pharmaceutics*, 2022, **14**, 2660.
10 H. Zhang, *Ice Templating and Freeze-Drying for Porous Materials and Their Applications*, John Wiley & Sons, 2018.
11 L. Velichkina, Y. Barbashin and A. Vosmerikov, *Catal. Res.*, 2021, **1**, 1–12.
12 S. Mohebbi, M. Rostamizadeh and D. Kahforoushan, *Micropor. Mesopor. Mater.*, 2020, **294**, 109845.
13 R. Ellerbrock, M. Stein and J. Schaller, *Sci. Rep.*, 2022, **12**, 11708.
14 S. M. Al-Amsyar, *Micropor. Mesopor. Mater.*, 2022, **336**, 111896.
15 S. S. Shareef, A. Thaeir and O. Motea, *J. Surv. Fish. Sci.*, 2023, **10**, 5355–5367.
16 D. D. Ristiana, S. Suyanta and N. Nuryono, *Mater. Today Commun.*, 2022, **32**, 103953.
17 S. Dechakhumwat, P. Hongmanorom, C. Thunyaratchatanon, S. M. Smith, S. Boonyuen and A. Luengnaruemitchai, *Renew. Energy*, 2020, **148**, 897–906.
18 D. Liu, F. Qiu, N. Liu, Y. Cai, Y. Guo, B. Zhao and Y. Qiu, *Unconv. Resour.*, 2022, **2**, 139–157.
19 Y. Jia, Q. Shi, J. Wang, C. Ding and K. Zhang, *RSC Adv.*, 2020, **10**, 29618–29626.
20 M. Kot, R. Wojcieszak, E. Janiszewska, M. Pietrowski and M. Zieliński, *Mater.*, 2021, **14**, 968.